Journal of Molecular Structure 1176 (2019) 254–265

Contents lists available at ScienceDirect

Journal of Molecular Structure

journal homepage: http://www.elsevier.com/locate/molstruc

Synthesis, growth, structural, optical, thermal, laser damage threshold and computational perspectives of 4-nitrophenol 4-aminobenzoic acid monohydrate (4NPABA) single crystal

P. Karuppasamy [a, *], T. Kamalesh [a], V. Mohankumar [a], S. Abdul Kalam [b], Muthu Senthil Pandian [a], P. Ramasamy [a], Sunil Verma [c, d], S. Venugopal Rao [b]

[a] SSN Research Centre, SSN College of Engineering, Chennai 603110, Tamil Nadu, India
[b] Advanced Centre of Research in High Energy Materials (ACRHEM), University of Hyderabad, Gachibowli, Hyderabad, 500046, Telangana, India
[c] Laser Materials Development and Devices Division, Raja Ramanna Centre for Advanced Technology (RRCAT), Indore, 452013, Madhya Pradesh, India
[d] Homi Bhabha National Institute, Anushakti Nagar, Mumbai, 400094, Maharashtra, India

ARTICLE INFO

Article history:
Received 3 June 2018
Received in revised form
22 August 2018
Accepted 23 August 2018
Available online 28 August 2018

Keywords:
Slow evaporation solution technique
4NPABA crystal
X-ray diffraction
Optical transmittance
Thermal properties
Laser damage threshold
Z-scan
Gaussian

ABSTRACT

A new organic compound 4-nitrophenol 4-aminobenzoic acid monohydrate (4NPABA) was synthesized and crystals were grown by slow evaporation solution technique (SEST). The crystal structure of 4NPABA was confirmed by single crystal X-ray diffraction (SXRD) and it was found to be monoclinic system with the centrosymmetric space group $P2_1/c$. The powder XRD (PXRD) was carried out for analysis of diffracting planes of grown crystal and also indexed by the Rietveld refinement using FullProf code. The ^{1}H NMR and ^{13}C NMR spectral analysis was used to confirm the chemical environment of various protons and carbons present in a 4NPABA structure. The various functional groups of the grown crystal were identified using Fourier transform infrared (FTIR) and FT-Raman spectroscopy. The transmittance of the grown crystal was analyzed by using UV–Visible–NIR spectral analysis and the cut-off wavelength was found to be 400 nm. The thermal stability of the grown crystal has been investigated by TGA-DTA studies. Laser damage threshold (LDT) value of the grown crystals has been determined using a nanosecond (ns) Nd:YAG laser operating at 532 nm. The third-order nonlinear optical property of 4NPABA crystal was studied by Z-scan technique to determine its nonlinear absorption (β) and nonlinear refraction (n_2). The charge transfer characteristic of the grown crystal was studied by frontier molecular orbital (FMOs) analysis. The hydrogen bonding of the present molecule was confirmed by NBO analysis. The polarizability and hyperpolarizability of the 4NPABA were calculated at the B3LYP/6–311++G (d,p) level using Gaussian 09W package. The calculated values of linear polarizability (α^*) and first order hyperpolarizability (β^*) are 2.683×10^{-23} (esu) and 11.865×10^{-30} (esu) respectively.

1. Introduction

In recent years, search continues for organic single crystal for a large number of applications such as photonics, optical information processing, 3D optical memory storage, electro-optic switches, color display, frequency doubling and optoelectronics [1–3]. Therefore, synthesis of new organic compounds with large nonlinear optical co-efficient have attracted many research groups. Normally the organic compounds have potentially high polarized π conjugation systems and hence they have been found to possess large frequency conversion compared to its inorganic compounds. The π-conjugated organic systems have emerged as attracting candidates because of this high second and third-order optical nonlinearities (SHG, THG), high damage resistance and large electro-optic co-efficient [4,5]. 4-nitrophenol (4NP) is an interesting material, because of a simple phenolic compound, it contains both nitro (acceptor group) and a hydroxyl (donor group) in a benzene ring. The 4NP is a classic dipolar NLO chromophore and a donor- π -acceptor system (D-π-A) and hence the more possibility of proton transfer from the phenolic (OH) to various organic bases can result in increasing of its molecular hyperpolarizability [6]. This D-π-A structure is added advantage to convert the frequency of the

* Corresponding author. Tel: +91-9791552297.
E-mail addresses: karuppasamyp75@gmail.com, karuppasamyp@ssn.edu.in (P. Karuppasamy).

https://doi.org/10.1016/j.molstruc.2018.08.074
0022-2860/

light. 4-aminobenzoic acid (4ABA) is one of the well-known carboxylic acids to promoting molecular self-assembly by means of strong hydrogen bonding [7]. 4ABA is of considerable use in the formation of stable molecular adducts with other carboxylic acids, particularly via hydrogen bonding through the amino group. It is very important in the pharmaceutically acceptable agent of co-crystallization [8,9]. The molecule consists of an aromatic ring, an NH_2 substituent which is electron donating and a COOH substituent which is electron accepting during the reactions and hence 4ABA molecule has both accepting and donating abilities of strong hydrogen bonding [10] and also it has different polymorphic forms [11]. In this case, the two organic chromophores such as 4NP and 4-ABA were combined to the formation of co-crystallization (4NPABA) with one water molecule (H6A-O6-H6B), since they possess a typical linear D-π-A conjugated chain, and are prone to the formation of strong hydrogen bonds. Hydrogen bonding has become a crucial part of the crystal engineering strategy with synthons, or recognizable robust intermolecular interaction motifs, being at the forefront. Thus examining the hydrogen bonding capability of a molecule may provide information relevant to assessing the likelihood of polymorphism [10–13]. The 4NP is bonded to the bridge of O3···H6A-O6 and the nitro group of 4ABA is directly involved to bonding in the conjugated chain of N2···H6B–O6. The combination of these chains (N2···H6A-O6-H6B···O3) together form a three-dimensional network. Generally, optical limiting property exhibited by organic molecules is related to high delocalization of the π-electrons. The optical limiting behavior resulting from nonlinear absorption can occur due to reverse saturable absorption, two-photon absorption, nonlinear refraction and nonlinear scattering [14]. Unlike second-order materials, there exist no molecular symmetry restrictions for the observance of a third-order nonlinear optical response.

In the present work, we have attempted to grow a novel single crystal of 4-nitrphenol 4-aminobenzoic acid monohydrate (4NPABA) by slow evaporation solution technique (SEST). The grown crystals were characterized by single crystal X-ray diffraction, Powder X-ray diffraction, ^{1}H and ^{13}C NMR, Fourier transform infrared (FTIR), FT-Raman, UV–Vis NIR, thermogravimetric (TG) and differential thermal analysis (DTA), laser damage threshold (LDT) and Z-scan analysis. In addition to these studies, optimized molecular structure, FMOs, linear polarizability, first-order hyperpolarizability, Mulliken charge analysis and NBO of the 4NPABA molecule were performed by DFT method for the first time in literature.

2. Synthesis, crystal growth and morphology

The 4NPABA compound was synthesized by using commercially available AR grade 4-nitrophenol and 4-aminobenzoic acid with molar ratio of 1:1 in a methanol solvent. The solution was continuously stirred until it became homogenous. The prepared solution was filtered by using Whatman filter paper and then poured into the crystallizing dish. The crystallizing dish was covered by the polythene sheet and a few tiny holes were made for making controlled evaporation at room temperature. After a few days, the dark yellow colored 4NPABA single crystals were randomly formed in a crystallizing dish. The synthesized material was further purified by repeated recrystallization process. The good quality of 4NPABA single crystals have been grown in a period of 30 days. The reaction mechanism of the synthesized 4NPABA material is depicted in Fig. 1. The photographs of as-grown 4NPABA crystals are shown in Fig. 2. The morphology of 4NPABA was indexed by WinXMorph software program. The indexed morphology of 4NPABA is shown in Fig. 3.

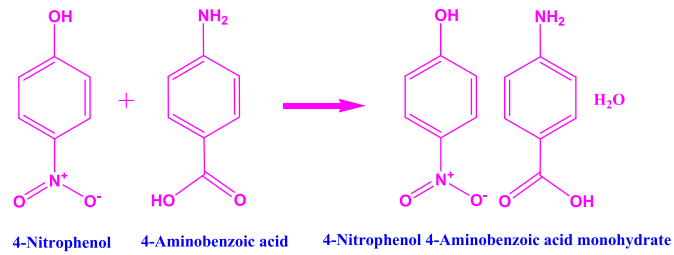

Fig. 1. Reaction scheme of 4NPABA.

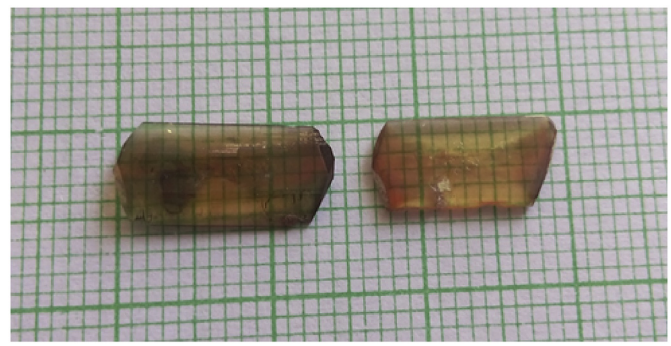

Fig. 2. As grown 4NPABA single crystals.

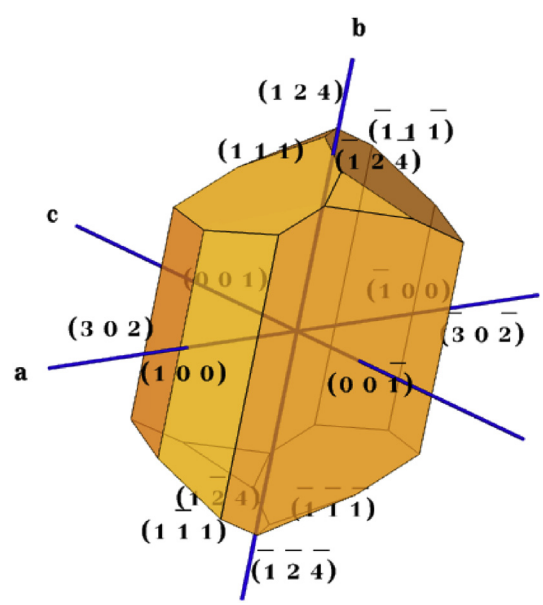

Fig. 3. Morphology of 4NPABA.

2.1. Solubility

The solubility study was carried out as a function of temperature ranging from 30 °C to 60 °C with an interval of 10 °C using a constant temperature bath with an accuracy of ±0.01 °C. In order to study the solubility, the small amount of solute was slowly added to the methanol solvent and maintained at 30 °C with continuous stirring using immersible magnetic stirrer with controller. After attaining the saturation, the equilibrium concentration of the solution was analyzed gravimetrically. The same process was repeated for different temperature to determine the solubility. The quantity of dissolved salt increases with increasing temperature in

a given volume of solvent and hence it confirms the grown crystal has positive solubility nature. The positive solubility of 4NPABA is given in the Fig. 4.

2.2. Characterization techniques

The grown 4NPABA single crystal was subjected to various characterization studies. The Bruker AXS Kappa APEX II CCD Diffractometer, equipped with monochromatic MoK$_\alpha$ radiation ($\lambda = 0.710$ Å). The powder X-Ray diffraction studies were carried out using BRUKER X-ray diffractometer with the Cu K$_\alpha$ radiation ($\lambda = 1.5406$ Å). The NMR was carried out using Bruker AVANCE III 500 MHz (AV 500) multi nuclei solution NMR Spectrometer. FTIR spectrum of grown crystal was recorded using Bruker AXS FTIR spectrometer at room temperature in the range of 500–4000 cm^{-1} with method of KBr pellet technique. FT-Raman was carried out using BRUKER RFS 27: Standalone FT-Raman Spectrometer with scanning range 50–4000 cm^{-1}. The UV–Vis NIR spectrum for the 4NPABA crystal was recorded using Perkin-Elmer Lambda-35 spectrophotometer in the range of 200–1100 nm. The thermogravimetric and difference thermal analysis (TG-DTA) was carried out between 30 °C and 370 °C at a heating rate of 10 °C/min in the nitrogen atmosphere using a Perkin-Elmer Diamond TG-DTA instrument. Laser damage threshold (LDT) was performed using a Q-switched Nd:YAG nanosecond laser (INNOLAS Spit Light, 1.2 J) at 1064 nm, 10 Hz, ~7 ns pulse duration. Z-scan studies was carried using a diode laser (100 mW) with wavelength of 532 nm.

3. Results and discussions

3.1. X-ray diffraction analysis

The suitable size of grown crystal was selected and subjected to single crystal X-ray diffraction (XRD) analysis. The crystal structure was solved by direct methods using SHELXS-97 and refined by full-matrix least squares against F^2 using SHELXL-97 software programme [15]. It reveals that the grown crystal crystallizes in the monoclinic crystallographic system and it has centrosymmetric space group $P2_1/c$ and R-factor equal to 0.0380. Full crystallographic data (CIF file) relating to the crystal structure of 4NPABA has been deposited with the Cambridge Crystallographic Database (CCDC 1457375). The crystallographic data of 4NPABA is given in Table 1. The hydrogen bondings of 4NPABA are given in the S. Table 1. A view of the 4NPABA complex with the atomic numbering scheme is depicted in ORTEP and shown in Fig. 5 and the crystal packing diagram is shown in S. Fig. 1. The PXRD was carried out at room temperature in order to check the phase purity. The obtained PXRD pattern for 4NPABA is in good agreement with that of Rietveld refinement using the FullProf code performed on the 2θ scans from 10° to 80° and CIF data. The obtained peaks have been indexed and are shown in Fig. 6. The well-defined peaks appeared corresponding to the angles (2θ) and it shows a high degree of crystallinity of 4NPABA crystal. The growth morphology of 4NPABA was generated and indexed by using a single crystal XRD data (CIF format) given as input to the WinXMorph software program [16].

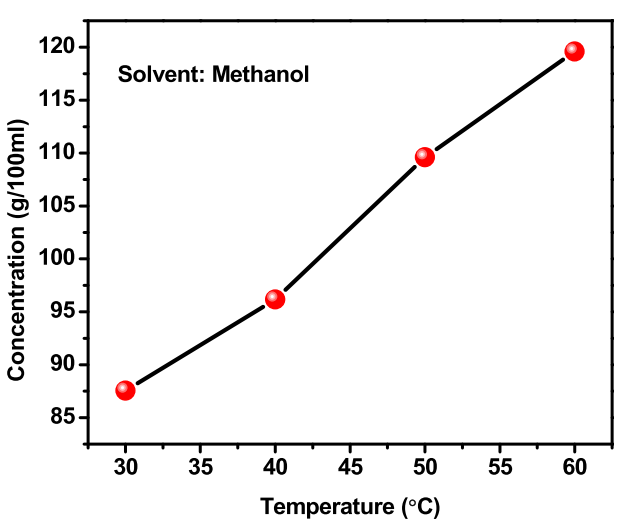

Fig. 4. Solubility curve of 4NPABA as a function of temperature.

Table 1
Crystallographic data for 4NPABA crystal.

Parameters	Description	
Identification code	4NPABA	
CCDC	1457375	
Empirical formula	$C_{13}H_{14}N_2O_6$	
Formula weight	294.26 g/mole	
Temperature	296 (2) K	
Wavelength	0.71073 Å	
Crystal system	Monoclinic	
Space group	$P2_1/c$	
Unit cell dimensions	a = 12.2560 (6) Å	$\alpha = 90°$
	b = 6.1232 (2) Å	$\beta = 90.318$ (2)°
	c = 18.5364 (7) Å	$\gamma = 90°$
Volume (V)	1391.06 (10) Å^3	
Z	4	
Density (ρ)	1.405 Mg/m^3	
Absorption co-efficient	0.113 mm^{-1}	
F (000)	616	
Crystal size	0.350 × 0.300 × 0.250 mm^3	
Theta range for data collection	2.197–25.000°	
Index ranges	$-14 \le h <= 14$, $-7 \le k <= 7$, $-22 \le l <= 22$	
Reflections collected	16710	
Independent reflections	2462 (R (int) = 0.0312)	
Completeness to theta = 25.000°	100.00%	
Absorption correction	Semi-empirical from equivalents	
Max. and min. transmission	0.987 and 0.957	
Refinement method	Full-matrix least-squares on F2	
Data/restraints/parameters	2462/6/207	
Goodness-of-fit on F2	1.104	
Final R indices [I > 2sigma(I)]	R1 = 0.0380, wR2 = 0.0927	
R indices (all data)	R1 = 0.0564, wR2 = 0.1109	
Extinction co-efficient	0.033 (2)	
Largest diff. peak and hole	0.211 and −0.233 e.Å^{-3}	

3.2. ^{1}H and ^{13}C NMR studies

The ^{1}H and ^{13}C nuclear magnetic resonance (NMR) spectral analysis is an important analytical technique used to the study of the organic compounds. It is also an important tool to identify the molecules and examine their functional groups in a structure. The NMR studies were carried out with Dimethyl sulfoxide (DMSO-d_6) as a solvent. The ^{1}H and ^{13}C NMR spectra of 4NPABA are given in Fig. 7 and Fig. 8 respectively. The corresponding peaks are assigned and tabulated (S. Table 2). In proton NMR spectrum, the hydrogen atoms are present in the various chemical environment. The major peaks arise between δ = 6.5 ppm–8 ppm, it indicates the presence of carbon-hydrogen (C–H) in an aromatic (benzene) ring. The doublet at δ = 7.6 ppm and 6.5 ppm represents the four protons are

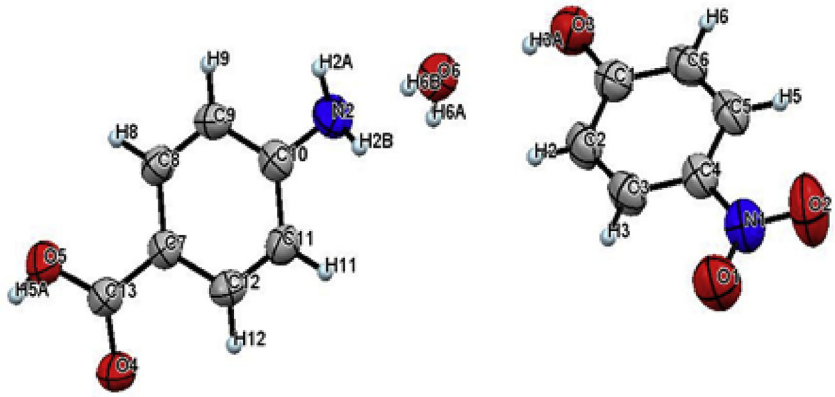

Fig. 5. Molecular structure (ORTEP) of 4NPABA.

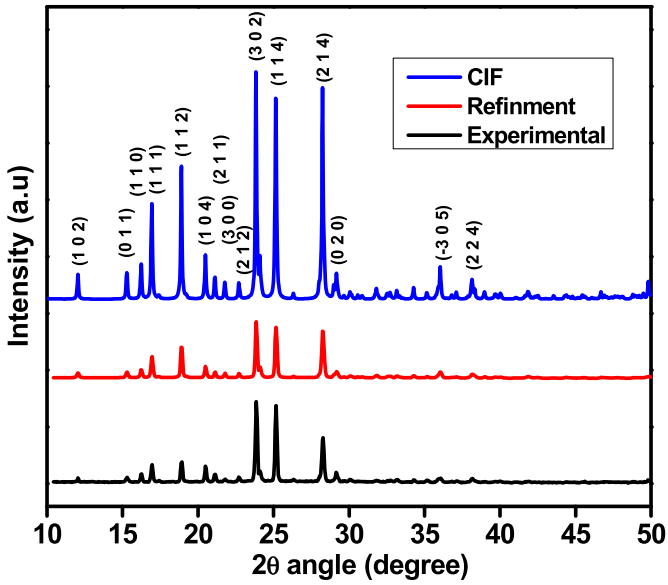

Fig. 6. The powder XRD spectra of 4NPABA.

C8–H8, C12–H12 and C9–H9, C11–H11 of the aromatic carbons in a 4ABA molecule. The two aromatic group signal is split into a multiplet due to the hyperfine splitting of neighboring protons. The doublet at $\delta = 8.1$ ppm and 6.9 ppm represents the four protons C2–H2, C6–H6 and C3–H3, C5–H5 of the aromatic carbons in 4NP molecule. The broad singlet at $\delta = 11.89$ ppm and 11.14 ppm indicates the hydrogen (H5A) atom in the carboxylate (COOH) group and hydrogen (H3A) atom in the hydroxyl (OH) group respectively. The singlet at $\delta = 5.8$ ppm represents the hydrogen (H2A-N2-H2B) present in an amine group. The singlet at $\delta = 3.44$ ppm indicates the presence of water molecule (H6A-O6-H6B) in a grown crystal.

In ^{13}C spectra, the signal of $\delta = 131.69$ ppm and 116.27 ppm represents the set of aromatic carbon in a 4ABA environment such as C12–H12, C8–H8 and C11–H11, C9–H9 respectively. And the further signals are due to C7 and C13 which give the corresponding shift of $\delta = 117.38$ ppm and 167.98 ppm in a 4ABA respectively. The aromatic ring of 4NP gives the chemical shift of 131.6 ppm and 113.2 ppm for the C6–H6, C2–H2 and C5–H5, C3–H3 respectively. The singlet of 164.35 ppm and 140.09 ppm is due to the carbon of C1 and C4 in the 4NP aromatic ring respectively.

3.3. FT-IR and FT-Raman spectral analysis

Vibrational spectroscopy is an important tool for understanding the chemical bonding and the presence of various functional groups in the material. FTIR spectrum of grown crystal was recorded using Bruker AXS FTIR spectrometer and it was carried out at room temperature in the range of 500–4000 cm^{-1} with KBr pellet technique. FT-Raman was carried out using BRUKER RFS 27: Standalone FT-Raman Spectrometer. The FTIR and FT-Raman spectra are shown in Fig. 9 and Fig. 10, respectively. The spectral range is 4000–50 cm^{-1} with resolution of 2 cm^{-1} using an Nd: YAG 1064 nm laser source. A peak around 3448 and 3405 cm^{-1} are observed due to the NH_2 asymmetric and symmetric stretching vibrations. It confirms the presence of 4-aminobenozic acid in grown 4NPABA crystal. The peak at 3320 cm^{-1} represents O–H stretching, which is absent in the FT-Raman spectrum. The broadening of the peak (2500-3000 cm^{-1}) is due to presence of C–H stretching rich in the present crystal. The unresolved vibrations are clearly resolved at 3077.02 cm^{-1} in FT-Raman spectrum. The strong peak at 1675 cm^{-1} is due to the presence of carboxylic acid (COOH), hence it confirms the presence of 4-aminobenzoic acid. On the other hand, this vibration has not been observed in FT-Raman spectrum. The peak at 1600 cm^{-1} is due to the aromatic skeleted stretching of vibration C=C and also which is present at 1603.45 cm^{-1} in FT-Raman. The 1550–1680 cm^{-1} regions of the FT-Raman spectra of the complexes contain the phenyl C=C stretching mode. This peak at 1603.45 cm^{-1} is assigned to the aromatic stretching vibration. The peak at 1496 cm^{-1} is the asymmetric stretching vibration of aromatic nitro (NO_2) group and it is present in FT Raman at 1496.24 cm^{-1}. The benzene ring has two or three bands in this region due to skeletal vibrations, the peak usually being at about 1496.24 cm^{-1}. The peak at 1420 cm^{-1} is due to C–C stretching in an aromatic ring, which does not appear in FT-Raman. The peak at 1335 cm^{-1} is due to the N=O strong symmetric stretching vibration of aromatic nitro group and it is present in FT-Raman at 1332.61 cm^{-1} [17]. The peak at 1281 cm^{-1} is assigned to strong C–N stretching vibration of aromatic amine and also it is present in FT Raman at 1281.93 cm^{-1}. The peak at 1170 cm^{-1} confirms carboxylic acid (C–O) present in the material, it has weak band at 1163.64 cm^{-1} in FT-Raman. The bands around 1000 cm^{-1} are attributed to skeleton vibration of aromatic carbons. In the FT-Raman spectrum, such skeleton vibrations of aromatic carbons are very weak [18]. The intense peaks at 1110 cm^{-1} and 1109.08 cm^{-1} observed at IR and Raman spectra respectively are due to the C–NO_2 stretching vibrations. The peak at 942 cm^{-1} is assigned to

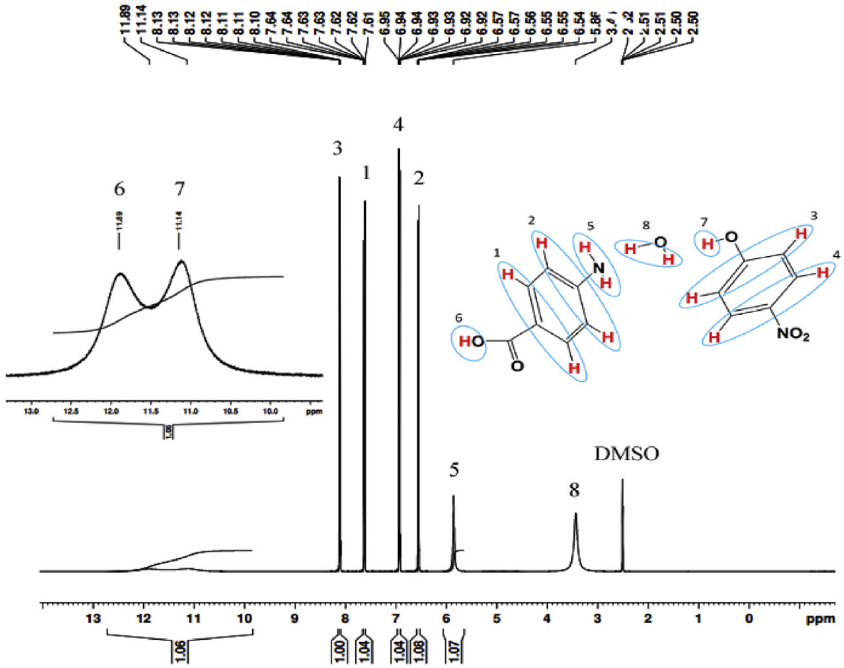

Fig. 7. ^{1}H NMR spectrum of 4NPABA.

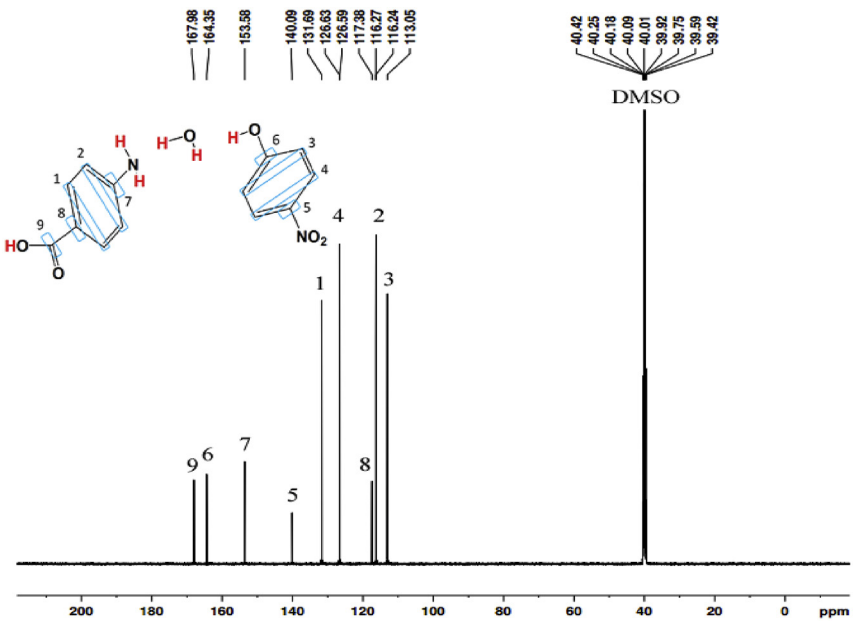

Fig. 8. ^{13}C NMR spectrum of 4NPABA.

O–H out of plane bending vibrations. The peak at 860 cm^{-1} and 864.57 cm^{-1} observed in IR and Raman spectra respectively indicate the C–H out-of-plane bending for 1,4-disubstituted benzene ring. The out-of-plane bending vibration of N–H group occurred at 795 cm^{-1}. In and out-of-plane bending of O–H showed their peaks at 753 cm^{-1}. The peaks at 690 cm^{-1}, 615 cm^{-1} and 550 cm^{-1} are represent wagging, scissoring and out of plane deformation of NO_2. In general, organic nitro compounds have a very strong band at 655-605 cm^{-1} due to the deformation vibration of the NO_2 group and corresponding Raman peak appeared at 637.73 cm^{-1}. The FTIR and FT-Raman spectra peaks assignments of 4NPABA are given in the S. Table 3.

3.4. UV–vis NIR spectral analysis

Optical transmittance spectrum of 4NPABA crystal was recorded in the wavelength range 200–1100 nm at room temperature. It gives the information about the structure of the molecule because the absorption of UV and visible light involves electronic transitions from bonding (σ and π) orbitals to anti-bonding (σ^* and π^*) orbitals [19]. The optical transmittance spectrum of 4NPABA crystal is shown in Fig. 11 (a). The lower cut-off wavelength was found to be at 400 nm, which indicates that the energy of 400 nm is required for the promotion of electrons from ground state to excited energy state due to absorptions. The dependence of the absorption co-

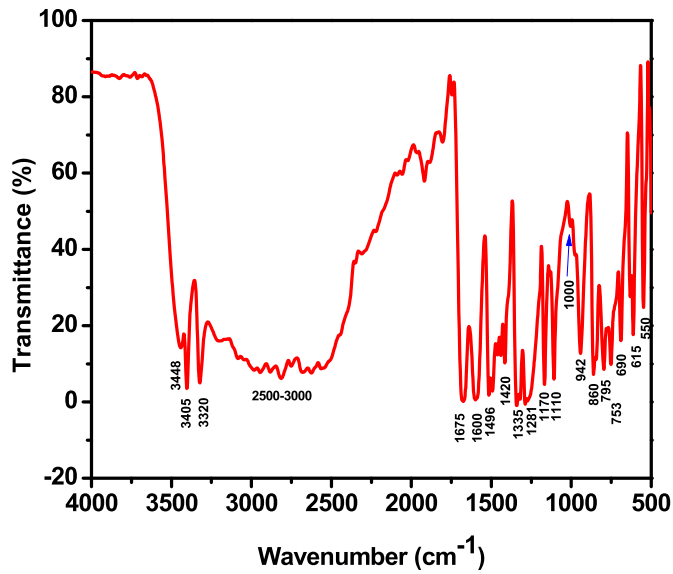

Fig. 9. FTIR spectrum of 4NPABA.

efficient as a function of photon energy is useful to study the band structure and transition of electrons. The linear optical absorption co-efficient (α) can be calculated by using the following relation:

$$\alpha = \frac{2.3026}{t}\log_{10}\left(\frac{100}{T}\right) \times \left(10^3\right)(\mathrm{m}^{-1}) \tag{1}$$

where T is the transmittance (%) and t is the thickness of the sample (2.5 mm). The quantity α (υ) can be displayed in a number of ways as described by the Tauc's plot relation [20]:

$$(\alpha h\upsilon) = A\left(h\upsilon - E_g\right)^m \tag{2}$$

where α is the absorption co-efficient, $h\upsilon$ is photon energy, E_g is the optical energy band gap, A is a constant and m is the characteristics of transition. The basic principle behind the technique is that the absorption of photons happens when their energy is equal or greater than the band gap of the materials. Therefore, the carriers undergoing transition from occupied state to unoccupied state by the two kinds of allowed transitions such as direct (no phonon interaction) and indirect (involves phonon interaction), and also these possess forbidden transitions. The transition number (m) is 1/2 for direct allowed transition, 2 for indirect allowed transition, 3/2 for direct forbidden transition and 3 for indirect forbidden transition [21,22]. In this case, we have to determine the value of 'm' to know the optical transition nature of 4NPABA crystal. Taking logarithm on both sides and differentiating the equation (2) with respect to $h\upsilon$ we get the following form:

$$\frac{d(\ln(\alpha h\upsilon))}{d(h\upsilon)} = \frac{m}{(h\upsilon - E_g)} \tag{3}$$

The value of E_g can be calculated from a graph plotted between $(\ln(\alpha h\upsilon))/h\upsilon$ and $h\upsilon$ which is shown in Fig. 11 (b). It gives a discontinuity at a particular maximum value and is found to be $E_g = 3.05$ eV. Plotting the graph between $(\ln(\alpha h\upsilon))$ and $(\ln(h\upsilon - E_g))$ the value of 'm' is obtained. The value of 'm' was found to be $0.429 \approx 0.5 = 1/2$ by extrapolating linear fit as shown in Fig. 11 (c). This confirms that the optical transition of 4NPABA crystal is of allowed direct band gap nature. Tauc's plot relation has been rearranged as given below for direct allowed transition:

$$(\alpha h\upsilon) = A\left(h\upsilon - E_g\right)^{\frac{1}{2}} \tag{4}$$

A graph is plotted between photon energy $(h\upsilon)$ and $(\alpha h\upsilon)^2$. By extrapolating the linear portion of the curve to zero absorption as shown in Fig. 11 (d), the optical band gap (E_g) of 4NPABA crystal was found to be 3 eV.

According to Planck's relation the energy of a photon (E) is proportional to its frequency and hence theoretically the optical band gap energy of 4NPABA crystal can be calculated using the following relation:

$$E_g = \frac{1240}{\lambda} eV \tag{5}$$

where λ is the lower cut-off wavelength (405 nm). The band gap of the grown 4NPABA crystal is found to be 3.06 eV, which is in good agreement with the value obtained from Fig. 11 (d).

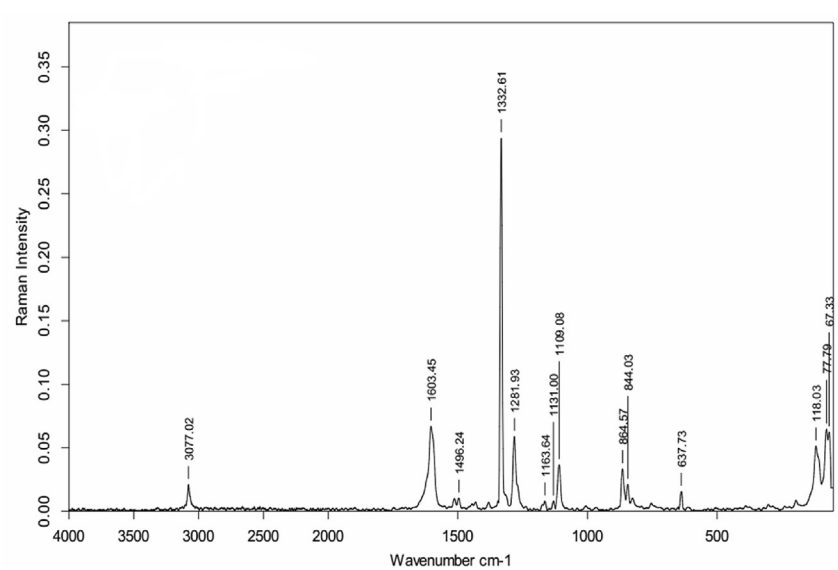

Fig. 10. FT-Raman spectrum of 4NPABA.

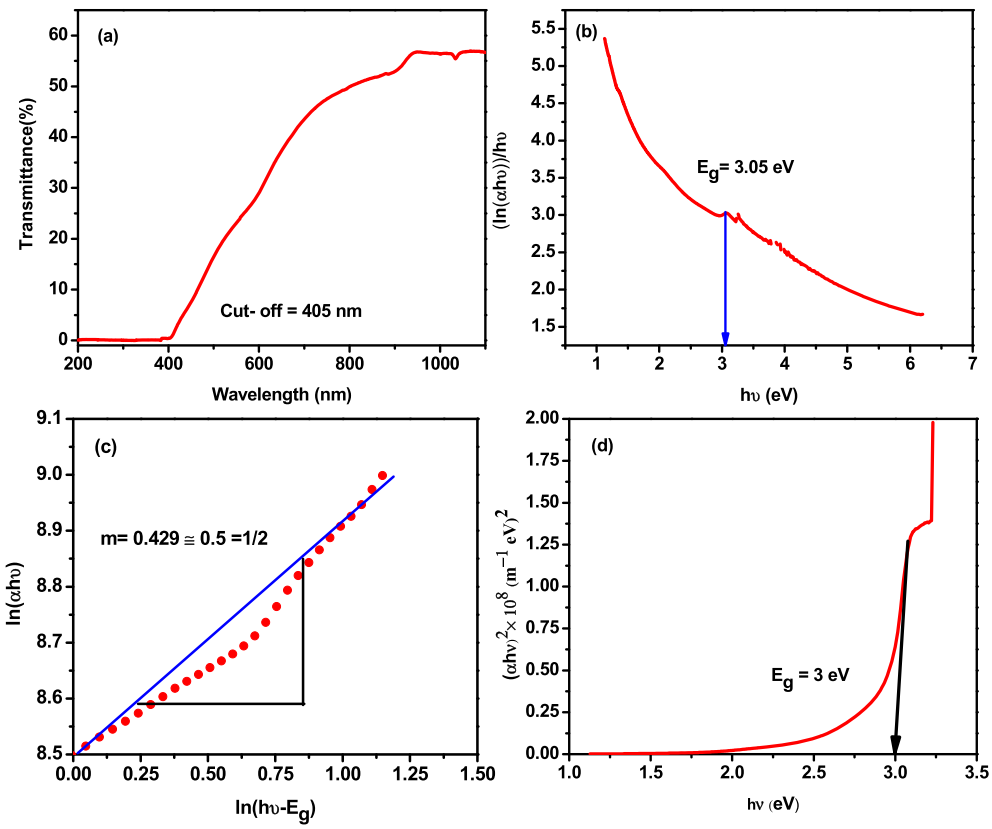

Fig. 11. (a) UV–Vis NIR spectrum, (b) Plot of (ln ($\alpha h\upsilon$))/$h\upsilon$ vs. $h\upsilon$ (c) Plot of (ln ($\alpha h\upsilon$)) vs. (ln($h\upsilon$ - E_g)) and (d) Optical band gap (E_g) spectrum of 4NPABA single crystal.

3.5. Thermogravimetric and differential thermal analysis

The thermal stability of 4NPABA crystal has been studied by thermogravimetric analysis (TGA) and differential thermal analysis (DTA). The 4NPABA powder sample was heated in the range of 30 °C–300 °C with the heating rate of 10 °C/min. It provides reliable information of sample about the charge of mass changes with respect to the temperature. The TG and DTA graph is shown in Fig. 12. In the TGA curve, it was observed that the initial weight loss of 10% around temperature increase from 80 °C to 155 °C is due to the liberation of weekly volatile substances like water molecules. It is confirmed that below this temperature there is no weight loss or phase transitions observed in the material. Weight loss of 94.5% occurs in a single stage between 155 °C and 235 °C. The DTA plot gives two endothermic peaks. The peak at 90 °C is due to the first stage of decomposing point of the 4NPABA and another endothermic peak noticed at 220 °C is due to second stage of bulk decomposition of the crystal. Finally, the residual masses of materials, around 5.4%, which remain may be carbons. Comparison of TGA and DTA results indicates that the crystal is stable up to 80 °C without any decomposition of the crystal. Hence, the suitability for optical device applications of the crystal is limited up to a temperature 80 °C.

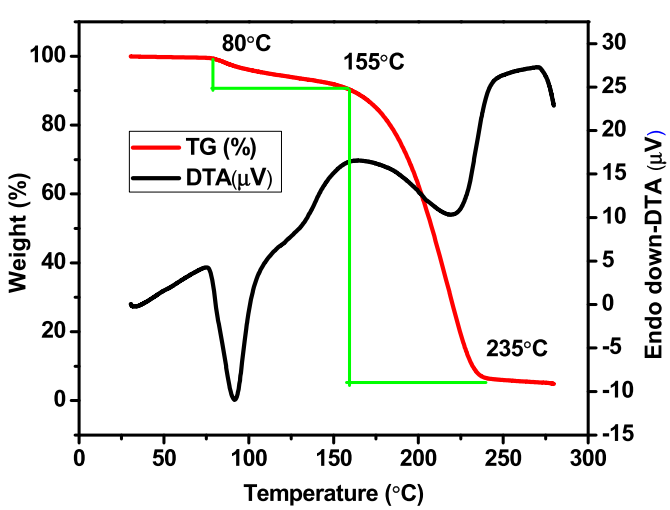

Fig. 12. TG-DTA of 4NPABA crystal.

3.6. Laser damage threshold (LDT) analysis

The high optical surface damage tolerance is extremely important characteristic of a NLO crystal for optoelectronic device applications. The laser damage threshold (LDT) of the NLO components depends on physical and chemical imperfections particularly on growth dislocations. The crystals containing several dislocations exhibit lower damage thresholds as these dislocations reduce the strength of interatomic bonds [23]. LDT study of 4NPABA crystal was performed using a Q-switched Nd:YAG nanosecond laser (INNOLAS Spit Light, 1.2 J @ 1064 nm, 10 Hz, ~7 ns pulse duration, input beam diameter of 8 mm) operating in transverse mode (TM_{00}) at 532 nm in the single shot mode. Experimental setup and other details can be found elsewhere [24]. The nanosecond pulses were focused by a plano convex lens of 10 cm focal length, which is attached to a translational stage and can be moved towards or away (Z direction, along the laser) from the sample. The crystal surface was interrogated 5 mm above from the focus and translated in X-Y plane using translational stages controlled by ESP

300. The output of the incident laser beam was controlled by an attenuator (combination of half-wave plate and Brewster's polarizer). The input laser energy density was recorded by a digital power meter. The single shot input laser energy was increased until the sample got damaged. The interrogation of laser causes localized heating due to absorption of photons by the material resulting in its vaporization, local melting as well as fracture from thermal stress [25]. However, the onset of laser induced damage depends on several factors such as absorption mechanism, material properties, presence of defects and incident laser wavelength and its pulse duration [26]. The input energy (mJ) was varied as 5, 10, 15, 20, 30 and 40 mJ. S. Fig. 2 depicts the laser induced damaged portions on surface of 4NPABA crystal. No damage (either crack or spot) was observed at 5 mJ and 10 mJ of input energy. A spot was initiated at 15 mJ and upon further increase in input energy, a visible damage at 40 mJ was observed. The surface damage threshold of the grown 4NPABA crystal was calculated using the following expression.

$$\text{Power density}(\mathrm{P_d}) = \frac{E}{\tau\pi(\omega_Z)^2} \tag{6}$$

where, E is the input pulse energy (mJ), τ is the pulse width (7 ns), and ω_z is the radius of the focused beam on crystal which is at 5 mm above the focal point and it is denoted as Z. The ω_z can be calculated using following expressions:

$$\omega_Z = \omega_0\sqrt{1+\left(\frac{Z}{Z_R}\right)^2} \tag{7}$$

$$Z_R = \left(\frac{\pi\omega_0^2}{\lambda}\right) \quad ; \ \omega_0 \geq \frac{2\lambda}{\pi} \tag{8}$$

$$2\omega_0 = \left(\frac{4\lambda}{\pi}\right)\left(\frac{f}{d}\right) \tag{9}$$

where λ is the wavelength of laser (532 nm), f is the focal length of convex lens (10 cm) and d is the diameter of laser beam (8 mm). The theoretical value of ω_o was estimated to be 4.23 μm. However, the experimental value was estimated from knife edge technique and was found to be ~10 μm. The Rayleigh length (Z_R) was found to be 590 μm and also condition of $\omega_0 \geq 2\lambda/\pi$ was satisfied. To avoid large peak intensities, the crystal was placed at a distance of 5 mm away from the focus for all the damage threshold studies. The radius of beam spot (ω_z) at a distance 5 mm away from focus was estimated using equation (7) and it was found to be ~85.3 μm. The calculated laser damage threshold value of 4NPABA crystal is 9.37 GW/cm^2 (15 mJ laser power). The crystal got severely damaged at 25.01 GW/cm^2 (40 mJ laser power).

3.7. Z-scan studies

The third order susceptibility of the grown 4NPABA crystal was investigated using Z-scan technique [27,28]. Materials with large third-order optical nonlinearity and fast response time are essential for future optical device applications in optical computing, real time holography, optical correlators and phase conjugators [29]. The Z-scan is defined as the plot of the relative power transmitted through the sample as a function of sample position. When the sample is placed far away from the focus there are no nonlinear processes present in the sample because of the low intensity of the light. When the sample is moved closer to the focus the intensity within the sample is increased leading to nonlinear processes. Therefore the transmittance of the samples is essential for this experiment. Nonlinear refractive and nonlinear absorptive phenomena in a sample give rise to characteristic features in the associated Z-scan traces [27]. Due to the above reasons the solid sample of 4NPABA is very difficult to use in an experiment, because transmittance at 532 nm is low (20%) (Fig. 11 (a)). Another way to improve the transmittance and finding the nonlinear parameter of the samples is by preparing the solution and also in different molar concentration such as 0.10 M 0.15 M, 0.20 M, 0.25 M and 0.30 M. The optical transmittance (T %) and linear refractive index (n_0) in different molar concentrations are shown in the S. Fig. 3 and S. Fig. 4 respectively. In this experiment, the diode laser (100 mW) with wavelength of 532 nm was used as a source and the beam diameter is 4 mm. The polarized Gaussian beam (TEM_{00}) was focused by a convex lens (focal length 200 mm) to produce the beam waist $\omega_o = 16.94$ μm. The thickness of the sample (L) was 1 mm (holder inner diameter). The Rayleigh length (Z_R) was calculated as 1.69 mm. The thickness of the samples must be less than the Rayleigh length and it was satisfied $(L < Z_R)$. All the Z-scan measurements were carried out at room temperature. The sample was mounted on a translation stage (at 90°) that was controlled by the computer to move along the negative $(-Z)$ to positive $(+Z)$ axis with respect to the focal point. When determining both sign and magnitude of the nonlinear refraction, an aperture (radius is 1.5 mm) was placed in front of the transmission detector and the transmittance was recorded as a function of the sample position on the Z axis (closed-aperture Z-scans). For measuring the nonlinear absorption, the Z-dependent sample transmittance was taken without the aperture (open-aperture Z scan) [30]. The schematic diagram of Z-scan setup is shown in Fig. 13 and The Z-scan experimental parameters are given in the S. Table. 4.

The intensity of a laser beam directly depends on the refractive index of the materials and its absorption nature. The sample causes an additional focusing or defocusing, depending on the nonlinear refraction values. As the sample traverses through the beam focus (at Z = 0), self-focusing or defocusing modifies the wave front phase, thereby modifying the transmitted beam intensity. However, the closed aperture Z-scan curve with pre-focal valley and post-focal peak indicates a self-focusing process and it is a positive sign for nonlinear refraction or self-defocusing process (pre-focal peak and post-focal valley) and it is a negative sign [31]. In an open aperture, the transmittance decreases (at less intensities) when the sample moves closer to the focal point (Z = 0) resulting in two or multi photons absorption or reverse saturable absorption (RSA) and then saturation achieved (T = 1) when the sample moves away from the focus. When the sample moves closer to the focal point (Z = 0) the transmittance increases (at high intensities), which indicates that the sample causes saturable absorption (SA) and then again saturation achieved (T = 1) when the sample moves away from the focus. From the open aperture Z-scan spectrum the nonlinear absorption coefficient (β) was calculated [32]. Fig. 14 (a) and (b) depict the closed and open aperture Z-scan spectra of 4NPABA in different concentrations.

In order to find out the nonlinear refractive index (n_2) of 4NPABA crystal, the $\Delta T_{p\text{-}v}$ was calculated using the equation:

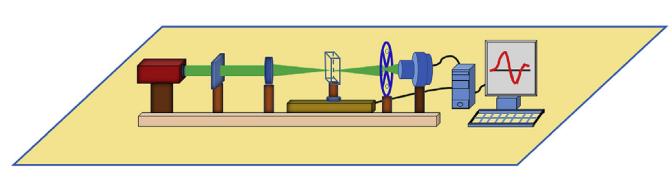

Fig. 13. The schematic diagram of Z-scan setup.

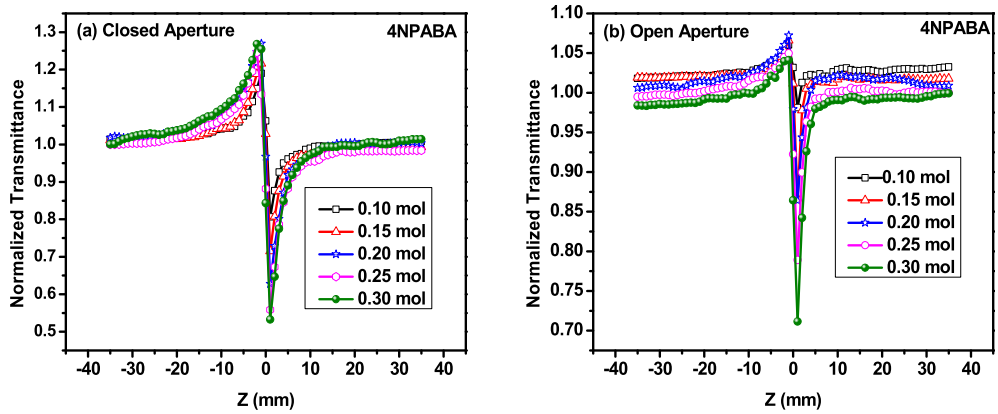

Fig. 14. (a) Closed and (b) open aperture Z-scan spectra of 4NPABA.

$$|\Delta\phi| = \frac{\Delta T_{p-v}}{0.406(1-S)^{0.25}} \tag{10}$$

where $\Delta\varphi$ is the axis phase shift at the focus, S is the linear transmittance aperture and it was calculated using the relation:

$$S = 1 - \exp\left(\frac{-2r_a^2}{\omega_a^2}\right) \tag{11}$$

where r_a is the radius of aperture (1.5 mm) and ω_a is the beam radius at the aperture (2.5 mm). The nonlinear refractive index (n_2) was calculated using the relation:

$$n_2 = \frac{\Delta\varphi}{kI_0L_{eff}}\left(m^2/W\right) \tag{12}$$

The nonlinear absorption coefficient (β) was determined using open aperture. The value of β would be positive for two or multiphoton absorptions and negative for saturable absorption (SA).

$$\beta = \frac{2\sqrt{2}\Delta T}{I_0L_{eff}}\ (m/W) \tag{13}$$

where k is the wave number $(k = 2\pi/\lambda)$, ΔT is the peak value at the open aperture Z − scan curve and I_0 is the intensity of the laser at the focus (0.11 MW/m^2). The effective thickness (L_{eff}) of the sample was calculated by using the following expression:

$$L_{eff} = \frac{1-\exp(-\alpha L)}{\alpha} \tag{14}$$

where α is the linear absorption coefficient and L is the thickness of the sample (1 mm). The effective thickness (L_{eff}) was found to be 0.99 mm. The real and imaginary parts of the third order nonlinear optical susceptibility $(\chi^{(3)})$ were estimated using the following relations [30]:

$$R_e\chi^{(3)}\ (esu) = \frac{10^{-4}\varepsilon_0c^2n_0^2n_2}{\pi}\left(cm^2/W\right) \tag{15}$$

$$I_m\chi^{(3)}\ (esu) = \frac{10^{-2}\varepsilon_0c^2n_0^2\lambda\beta}{4\pi^2}\ (cm/W) \tag{16}$$

where ε_0 is the vacuum permittivity (8.854×10^{-12} F/m), c is the velocity of light in vacuum (3×10^8 m/s), n_0 is the linear refractive index of the samples at 532 nm (S. Fig. 4). The third order nonlinear optical susceptibility of the grown crystal was calculated using the expression:

$$\chi^{(3)} = \sqrt{\left(R_e\chi^{(3)}\right)^2 + \left(I_m\chi^{(3)}\right)^2} \tag{17}$$

The calculated nonlinear refractive index (n_2), nonlinear absorption coefficient (β), real and imaginary parts of susceptibility and third-order nonlinear susceptibility $(\chi^{(3)})$ for 4NPABA with different molar concentrations are given in the Table 2. The obtained third-order nonlinear susceptibilities $(\chi^{(3)})$ increase with increasing concentration in the order of 10^{-9} (esu) and these are shown in Fig. 15. Increasing value of third-order nonlinear susceptibilities $(\chi^{(3)})$ is indicated that the grown crystals are more useful for NLO applications. The grown crystal has reverse saturable absorption (open aperture) and hence it is an ideal candidate for optical limiting applications [33]. The negative sign of the nonlinear refractive index (n_2) indicates the self-defocusing nature of the material. This may have an advantage in practical devices, by providing useful for the applications of holographic recording and two-wave mixing [34], photorefractive (PR) glasses, soliton wave communication [35], Self-trapping of light, as well as optically induced focusing-to-defocusing switching device applications [36].

3.8. Computational details

The quantum chemical calculations were employed with DFT method. All theoretical calculations are computed using Becke

Table 2
The nonlinear parameters of 4NPABA.

Con. (mol)	$(n_2) \times 10^{-12}$ (m^2/W)	$(\beta) \times 10^{-6}$ (m/W)	$R_e\ (\chi^{(3)}) \times 10^{-10}$ (cm^2/W)	$I_m\ (\chi^{(3)}) \times 10^{-9}$ (cm/W)	$(\chi^{(3)}) \times 10^{-9}$ (esu)
0.10	0.86	0.51	0.68	0.17	0.18
0.15	1.12	3.57	0.94	1.26	1.26
0.20	1.44	3.57	1.62	1.70	1.71
0.25	1.53	5.61	1.99	3.09	3.10
0.30	1.66	7.40	2.77	5.21	5.21

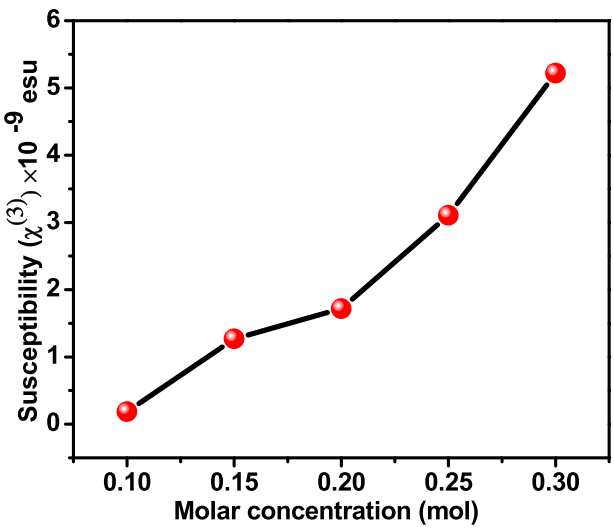

Fig. 15. Susceptibilities ($\chi^{(3)}$) in different molar concentrations.

three parameter Lee-yang-Parr (B3LYP) with 6–311++G (d,p) standard basis set [37]. The optimized molecular geometry of 4NPABA was selected for further calculations. The natural bond orbital analysis (NBO) of titled molecule was carried out with the same basis set [38]. The polarizability and other electronic properties of the isolated molecule were calculated with the same level of theory. All the calculations were employed using Gaussian 09 W program package [39].

3.8.1. Optimized molecular structure

The optimized molecular structure of 4NPABA molecule with atom numbering scheme was depicted in Fig. 16. The computed geometrical parameters were compared with available XRD data. The optimized geometrical parameters of band length and band angle are listed in S. Table 5 and S. Table 6 respectively. The discrepancies between computed and experimental values are due to the different hydrogen and carbon environment. The theoretical values are calculated in gaseous phase for isolated molecule and intermolecular interactions are in the crystalline state. The C–C bond lengths are in the range of 1.384 Å – 1.481 Å for B3LYP and 1.4 Å – 1.536 Å for XRD. The C26–C16 has the highest bond length compared to other bond lengths it is due to the acid group in the C26 atom. C–H bond lengths are in the range of 1.081 Å – 1.085 Å for B3LYP and 1.065 Å – 1.072 Å for XRD. All the C–H bond lengths are nearly same. The C–O bond lengths are C1–O14, C26–O29, C26 = O28 in B3LYP 1.361 Å, 1.361 Å, 1.209 Å and from XRD 1.429 Å, 1.421 Å, 1.257 Å respectively. The C–O bond lengths are different due the various environment of oxygen atom. The O–H, N–H, N–O and C–N bond lengths are nearly same.

3.8.2. Frontier molecular orbital (FMOs) analysis

The highest occupied molecular orbital (HOMO) and the lowest unoccupied molecular orbital (LUMO) are named as frontier molecular orbital. The electronic transition from the ground state to the first excited state is mainly described by an electron excitation from the highest occupied molecular orbital (HOMO) to the lowest unoccupied molecular orbital (LUMO). HOMO is an electron donor while LUMO is an electron acceptor that represents ability to obtain an electron. HOMO and LUMO are calculated using B3LYP/6-31G (d,p) and the 3D plots are illustrated in Fig. 17. The HOMO is localized on the 4-aminobenzoic acid monohydrate part and smaller density was in the OH part of the 4NP. The LUMO of the 4NPABA was delocalized over the 4NP part of the molecule. The HOMO–LUMO transition implies an electron density transfer from 4ABA ring to 4NP part of molecule. The energies of molecular orbitals of 4NPABA were calculated with same level of theory. The calculated energy values of the HOMO and LUMO are −6.582 eV and −2.992 eV respectively. The value of energy gap between the HOMO and LUMO is 3.59 eV in the gas phase.

3.8.3. Molecular electrostatic potential (MEP)

The molecular electrostatic potential (MEP) map of 4NPABA was depicted in Fig. 18. The region of most negative, most positive and zero electrostatic potential are represented by red, blue and green color respectively. The negative MEP is delocalized over the oxygen and nitrogen atoms and is reproduced by red and yellowish color respectively. The regions having the positive potential are delocalized over all hydrogen atoms. The concentrated electron density in the molecule attracted proton and it is corresponding to the negative electrostatic potential. The repulsion of proton by atomic nuclei corresponds to positive electrostatic potential. The MEP gives the molecular structure along with its physiochemical properties [40].

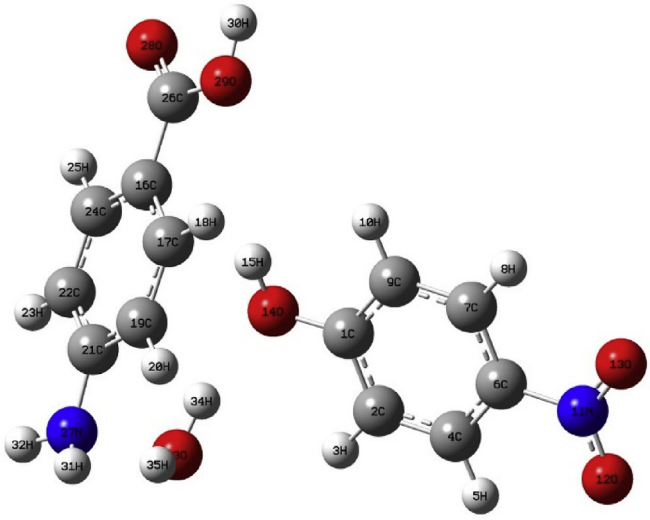

Fig. 16. Optimized molecular structure of 4NPABA.

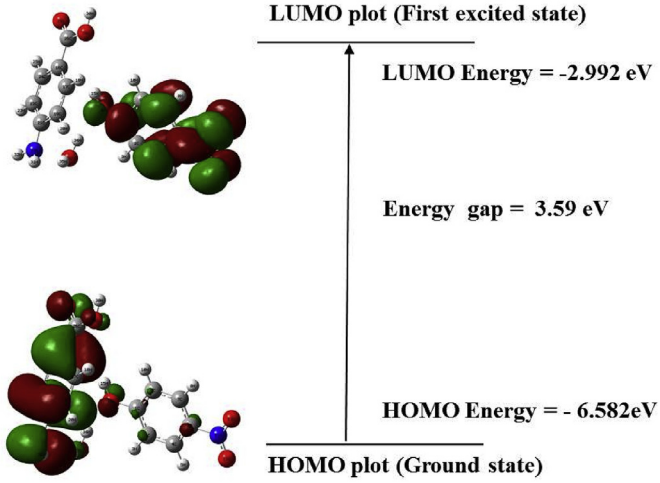

Fig. 17. Frontier molecular orbital (FMO) of 4NPABA.

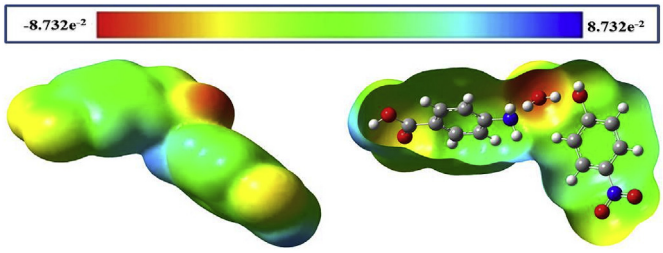

Fig. 18. Molecular electrostatic potential (MEP) map of 4NPABA.

3.8.4. Nonlinear optical studies

The molecular polarizability is an indicator of nonlinear optical response of an isolated molecule in external field $E_i(\omega)$. Where μ_0 is the permanent dipole moment, α^* is the linear polarizability and β^*_{ijk} are the first hyperpolarizability tensor components. Polarizability (α^*) and hyper polarizability (β^*) tensor components are given in S. Table 7.

The average linear polarizability is defined as

$$\alpha^*_{Tot} = \frac{(\alpha^*_{xx} + \alpha^*_{yy} + \alpha^*_{zz})}{3} \tag{18}$$

First hyper polarizability is third rank tensor that can be described by $3 \times 3 \times 3$ matrix. The 27 components are reduced to 10 components due to kleinman symmetry [41]. The output from Gaussian 09 provides 10 components of this matrix as β^*_{xxx}, β^*_{xxy}, β^*_{xyy}, β^*_{yyy}, β^*_{xxz}, β^*_{xyz}, β^*_{yyz}, β^*_{xzz}, β^*_{yzz}, β^*_{zzz} respectively. Using the x, y and z components the magnitude of the first hyperpolarizability tensor β^* can be calculated by

$$\beta^*_{Tot} = \left(\beta^{*2}_x + \beta^{*2}_y + \beta^{*2}_z\right)^{1/2} \tag{19}$$

The complete equation for calculating β^* is given as following equation

$$\beta^*_{Tot} = \left(\left(\beta^{*2}_x + \beta^{*2}_y + \beta^{*2}_z\right) + \left(\beta^{*2}_x + \beta^{*2}_y + \beta^{*2}_z\right) + \left(\beta^{*2}_x + \beta^{*2}_y + \beta^{*2}_z\right)\right)^{1/2} \tag{20}$$

The polarizability and hyperpolarizability of the titled compound were calculated at the B3LYP/6–311++G (d,p) level using Gaussian 09W package. The calculated value of linear polarizability (α^*) and hyperpolarizability (β^*) values are 2.683×10^{-23} e.s.u. and 11.865×10^{-30} e.s.u., respectively.

4. Conclusions

An organic single crystal, 4NPABA was successfully grown by slow evaporation solution technique and it belongs to the monoclinic system with centric space group, $P2_1/c$. The single crystal XRD (SXRD) was carried out to solve the crystal structure. Powder X-ray diffraction (PXRD) analysis shows a relatively good crystalline nature and also refined using FullProf code. The molecular structure of 4NPABA was recognized by NMR (^{1}H and ^{13}C) studies and its vibrational modes were confirmed by FTIR and FT-Raman studies. UV–Vis–NIR spectrum of grown crystal shows good optical transparency in the visible and near-IR region with cut-off wavelength 405 nm. The thermal stability of the grown crystal is upto 80 °C. The higher value of LDT indicates that the 4NPABA crystal is useful for laser applications. Z-scan study was made with different molar concentrations and confirms 4NPABA crystal has self-defocusing and reverse saturable absorption nature. The bonding interactions and charge transfer of title molecule were analyzed by Mulliken atomic charge and FMO's respectively. The calculated first order hyperpolarizability (β^*) value of 4NPABA was 23.9 times greater than that of urea. Third-order nonlinear optical susceptibilities ($\chi^{(3)}$) of 4NPABA were found to be in the order of 10^{-9} (esu). The higher value of β^* and $\chi^{(3)}$ indicated that the grown crystals are more useful for NLO applications. Also the grown crystal has reverse saturable absorption (open aperture) and hence it is useful for practical devices such as optical limiter, two-wave mixing and switching devices.

Acknowledgments

This work was supported by the BRNS project (Ref. 34/14/06/2016-BRNS/34032), Government of India. The authors are thankful to SAIF, IIT-Madras for single crystal XRD, NMR and Raman studies. S. Venugopal Rao thanks DRDO for financial support through ACRHEM for using LASER facility.

Appendix A. Supplementary data

Supplementary data related to this article can be found at https://doi.org/10.1016/j.molstruc.2018.08.074.

References

[1] M. Kitazawa, R. Higuchi, M. Takahashi, Ultraviolet generation at 266 nm in a novel organic nonlinear optical crystal: l-pyrrolidone-2-carboxylic acid, Appl. Phys. Lett. 64 (1994) 2477.
[2] W.S. Wang, M.D. Aggarwal, J. Choi, T. Gebre, A.D. Shields, B.G. Penn, D.O. Frazier, Solvent effects and polymorphic transformation of organic nonlinear optical crystal L-pyroglutamic acid in solution growth processes: I. Solvent effects and growth morphology, J. Cryst. Growth 198 (1999) 578–582.
[3] J.P. Zou, Q. Peng, Z. Wen, G.S. Zeng, Q.J. Xing, G.C. Guo, Two novel Metal–Organic frameworks (MOFs) with (3,6)-connected net topologies: syntheses, crystal structures, third-order nonlinear optical and luminescent properties, Cryst. Growth Des. 10 (2010) 2613–2619.
[4] K. Clays, B.J. Coe, Design strategies versus limiting theory for engineering large second-order nonlinear optical polarizabilities in charged organic molecules, Chem. Mater. 15 (2003) 642–648.
[5] M. González, J.L. Segura, C. Seoane, N. Martín, Tetrathiafulvalene derivatives as NLO-phores: synthesis, electrochemistry, Raman spectroscopy, theoretical calculations, and NLO properties of novel TTF-derived donor-π-acceptor dyads, J. Org. Chem. 66 (2001) 8872–8882.
[6] C.C. Evans, M. Bagieu-Beucher, R. Massse, J.-F. Nicoud, Nonlinearity enhancement by solid-state proton transfer: a new strategy for the design of nonlinear optical materials, Chem. Mater. 10 (1998) 847–854.
[7] T.F. Lai, R.E. Marsh, The crystal structure of p-aminobenzoic acid, Acta Crystallogr. 22 (1967) 885.
[8] N. Issa, S.A. Barnett, S. Mohamed, D.E. Braun, R.C.B. Copley, D.A. Tocher, S.L. Price, Screening for cocrystals of succinic acid and 4-aminobenzoic acid, Cryst. Eng. Commun. 14 (2012) 2454.
[9] D.E. Lynch, G. Smith, Molecular co-crystals of carboxylic acid. 1:1 adduct of 1,3,5-Trinitrobenzene with 4-aminobenzoic acid, Acta Crystallogr. C50 (1994) 2079–2089.
[10] S. Gracin, A.C. Rasmuson, Polymorphism and crystallization of p-aminobenzoic acid, Cryst. Growth Des. 4 (2004) 1013–1023.
[11] S. Gracin, M.U. Penttila, A.C. Rasmuson, Influence of ultrasound on the nucleation of polymorphs of p-aminobenzoic acid, Cryst. Growth Des. 5 (2005) 1787–1794.
[12] G. Wojcik, I. Mossakowska, Polymorphs of p-nitrophenol as studied by variable-temperature X-ray diffraction and calorimetry: comparison with m-nitrophenol, Acta Crystallogr. B. 62 (2006) 143–152.
[13] T. Imai, Y. Yokoyama, A. Sekine, H. Uekusa, Y. Ohashi, The 2-methoxyphenylhydrazone derivative of dehydroascorbic acid, Acta Crystallogr. E59 (2003) o1241–o1243.
[14] L. Vivien, N. Izard, D. Riehl, F. Hache, E. Anglaret, Optical limiting properties of suspensions of single-wall carbon nanotubes, AIP Conf. Proc. 685 (2003) 559.
[15] G.M. Sheldrick, SHELX97, University of Gottingen, Germany, 1997.
[16] W. Kaminsky, From CIF to virtual morphology using the WinXMorph program, J. Appl. Crystallogr. 40 (2007) 382–385.
[17] R.A. Ando, A.C. Borin, P.S. Santos, Saturation of the electron-withdrawing capability of the NO2 group in nitroaromatic Anions: spectroscopic and quantum-chemical evidence, J. Phys. Chem. 111 (2007) 7194–7199.
[18] S. Debrus, M.K. Marchewka, J. Baran, M. Drozd, R. Czopnik, A. Pietraszko, H. Ratajczak, L-lysine-L-tartaric acid: new molecular complex with nonlinear optical properties. Structure, vibrational spectra and phase transitions, J. Solid

State Chem. 178 (2005) 2880–2896.
[19] R. Boikess, Chemical Principles for Organic Chemistry, 2014.
[20] J. Tauc, R. Grigorovici, A. Vancu, Optical properties and electronic structure of amorphous germanium, Phys. Status Solidi B15 (1996) 627–637.
[21] M. Elahi, D. Souri, Study of optical absorption and optical band gap determination of thin amorphous TeO_2-V_2O_5-MoO_3 blown films, Indian J. Pure Appl. Phys. 44 (2006) 468–472.
[22] N. Chopra, A. Mansingh, G.K. Chadha, Electrical, optical and structural properties of amorphous V2O5 TeO2 blown films, J. Non-Cryst. Solids 126 (1990) 194–201.
[23] P. Karuppasamy, Muthu Senthil Pandian, P. Ramasamy, Sunil Verma, Crystal growth, structural, optical, thermal, mechanical, laser damage threshold and electrical properties of triphenylphosphine oxide 4-nitrophenol (TP4N) single crystals for nonlinear optical applications, Opt. Mater. 79 (2018) 152–171.
[24] S. Abdul kalam, N. Linga Murthy, P. Mathi, N. Kommu, A.K. Singh, S. Venugopal Rao, Correlation of molecular, atomic emissions with detonation parameters in femtosecond and nanosecond LIBS plasma of high energy materials, J. Anal. At. Spectrom. 32 (2017) 1535–1546.
[25] G. Anandha Babu, S. Sreedhar, S. Venugopal Rao, P. Ramasamy, Synthesis, growth, structural, thermal, linear and nonlinear optical properties of a new organic crystal: dimethylammonium picrate, J. Cryst. Growth 312 (2010) 1957–1962.
[26] M.S. Brown, C.B. Arnold, Fundamentals of laser-material interaction and application to multiscale surface modification, in: K. Sugioka, et al. (Eds.), Laser Precision Microfabrication vol. 135, Springer Series in Materials Science, 2010, pp. 91–120. Chapter 4.
[27] M. Sheik-Bahae, A.A. Said, T.H. Wei, D.J. Hagan, E.W. Van Stryland, Sensitive measurement of optical nonlinearities using a single beam, IEEE J. Quant. Electron. 26 (1990) 760–769.
[28] P. Karuppasamy, V. Sivasubramani, M. Senthil Pandian, P. Ramasamy, Growth and characterization of semi-organic third order nonlinear optical (NLO) potassium 3, 5-dinitrobenzoate (KDNB) single crystals, RSC Adv. 6 (2016) 109105–109123.
[29] H.P. Li, B. Liu, C.H. Kam, Y.L. Lam, W.X. Que, L.M. Gan, C.H. Chew, G.Q. Xu, Femtosecond Z-scan investigation of nonlinear refraction in surface modified PbS nanoparticles, Opt. Mater. 14 (2000) 321–327.
[30] P. Karuppasamy, M. Senthil Pandian, P. Ramasamy, S. Verma, Crystal growth, structural, optical, thermal, mechanical, laser damage threshold and electrical properties of triphenylphosphine oxide 4-nitrophenol (TP4N) single crystals for nonlinear optical applications, Opt. Mater. 79 (2018) 152–171.
[31] M. Sheik-Bahae, A.A. Said, E.W. Van Stryland, High-sensitivity, single-beam n_2 measurements, Opt. Lett. 14 (1989) 955–957.
[32] I. Bhattacharyya, S. Priyadarshi, D. Goswami, Molecular structure-property correlations from optical nonlinearity and thermal-relaxation dynamics, Chem. Phys. Lett. 469 (2009) 104–109.
[33] H.I. Elim, J. Yang, J.-Y. Lee, J. Mi, W. Ji, Observation of saturable and reverse-saturable absorption at longitudinal surface plasmon resonance in gold nanorods, Appl. Phys. Lett. 88 (2006), 083107.
[34] H.M. Shanshoola, M. Yahaya, W.M.M. Yunus, I.Y. Abdullah, Using Z scan technique to measure the nonlinear optical properties of PMMA/ZNO nanocomposites, Jurnal Teknologi 78 (2016) 33–38.
[35] G.A. Swartzlander Jr., D.R. Andersen, J.J. Regan, H. Yin, A.E. Kaplan, Spatial dark-soliton stripes and grids in self-defocusing materials, Phys. Rev. Lett. 66 (1991) 1583–1586.
[36] Z. Chen, M. Asaro, O. Ostroverkhova, W.E. Moerner, M. He, R.J. Twieg, Self-trapping of light in an organic photorefractive glass, Opt. Lett. 28 (2003) 2509–2511.
[37] C. Lee, W. Yang, R.G. Parr, Development of the Colle-Salvetti correlation-energy formula into a functional of the electron density, Phys. Rev. B 37 (1988) 785.
[38] E.D. Glendening, J.K. Badenhoop, A.E. Reed, J.E. Carpenter, J.A. Bohmann, C.M. Morales, F. Weinhold, NBO 5.0, Theoretical Chemistry Institute, University of Wisconsin, Madison, 2001.
[39] M.J. Frisch, G.W. Trucks, H.B. Schlegel, G.E. Scuseria, M.A. Robb, J.R. Cheeseman, G. Scalmani, V. Barone, B. Mennucci, G.A. Petersson, H. Nakatsuji, M. Caricato, X. Li, H.P. Hratchian, A.F. Izmaylov, J. Bloino, G. Zheng, J.L. Sonnenberg, M. Hada, M. Ehara, K. Toyota, R. Fukuda, J. Hasegawa, M. Ishida, T. Nakajima, Y. Honda, O. Kitao, H. Nakai, T. Vreven, J.A. Montgomery Jr., J.E. Peralta, F. Ogliaro, M. Bearpark, J.J. Heyd, E. Brothers, K.N. Kudin, V.N. Staroverov, R. Kobayashi, J. Normand, K. Raghavachari, A. Rendell, J.C. Burant, S.S. Iyengar, J. Tomasi, M. Cossi, N. Rega, J.M. Millam, M. Klene, J.E. Knox, J.B. Cross, V. Bakken, C. Adamo, J. Jaramillo, R. Gomperts, R.E. Stratmann, O. Yazyev, A.J. Austin, R. Cammi, C. Pomelli, J.W. Ochterski, R.L. Martin, K. Morokuma, V.G. Zakrzewski, G.A. Voth, P. Salvador, J.J. Dannenberg, S. Dapprich, A.D. Daniels, Ö. Farkas, J.B. Foresman, J.V. Ortiz, J. Cioslowski, D.J. Fox, Gaussian 09, Revision D.01, Gaussian, Inc., Wallingford CT, 2009.
[40] R.G. Pearson, Absolute electronegativity and absolute hardness of Lewis acids and bases, J. Am. Chem. Soc. 107 (1985) 6801–6806.
[41] D.A. Kleinman, Nonlinear dielectric polarization in optical media, Phys. Rev. 126 (1977) 1962–1979.